PNAS RESEARCH ARTICLE | IMMUNOLOGY AND INFLAMMATION OPEN ACCESS

Identification of a unique subset of tissue-resident memory CD4$^+$ T cells in Crohn's disease

Takehito Yokoi[a,b,c,1], Mari Murakami[a,b,1], Takako Kihara[d], Shigeto Seno[e], Mitsuru Arase[a,b], James Badger Wing[b,f], Jonas Nørskov Søndergaard[f], Ryuichi Kuwahara[g], Tomohiro Minagawa[g], Eri Oguro-Igashira[a,b], Daisuke Motooka[b,h,i], Daisuke Okuzaki[b,f,h,i], Ryota Mori[j], Atsuyo Ikeda[j], Yuki Sekido[j], Takahiro Amano[k], Hideki Iijima[k,l], Keiichi Ozono[c], Tsunekazu Mizushima[j,m], Seiichi Hirota[d], Hiroki Ikeuchi[g], and Kiyoshi Takeda[a,b,f,i,2]

Edited by Hiroshi Ohno, Rikagaku Kenkyujo Togo Seimei Ikagaku Kenkyu Center, Yokohama, Japan; received March 10, 2022; accepted November 30, 2022 by Editorial Board Member Tadatsugu Taniguchi

T cells differentiate into highly diverse subsets and display plasticity depending on the environment. Although lymphocytes are key mediators of inflammation, functional specialization of T cells in inflammatory bowel disease (IBD) has not been effectively described. Here, we performed deep profiling of T cells in the intestinal mucosa of IBD and identified a CD4$^+$ tissue-resident memory T cell (Trm) subset that is increased in Crohn's disease (CD) showing unique inflammatory properties. Functionally and transcriptionally distinct CD4$^+$ Trm subsets are observed in the inflamed gut mucosa, among which a CD-specific CD4$^+$ Trm subset, expressing CD161 and CCR5 along with CD103, displays previously unrecognized pleiotropic signatures of innate and effector activities. These inflammatory features are further enhanced by their spatial proximity to gut epithelial cells. Furthermore, the CD-specific CD4$^+$ Trm subset is the most predominant producer of type 1 inflammatory cytokines upon various stimulations among all CD4$^+$ T cells, suggesting that the accumulation of this T cell subset is a pathological hallmark of CD. Our results provide comprehensive insights into the pathogenesis of IBD, paving the way for decoding of the molecular mechanisms underlying this disease.

inflammatory bowel disease | T-cell immunity | tissue-resident T cell | mass cytometry | single-cell RNA-seq

Inflammatory bowel disease (IBD), which consists of Crohn's disease (CD) and ulcerative colitis (UC), involves chronic inflammation of the digestive tract. Accumulating evidence indicates the heterogeneity of IBD, exhibiting different genetic and environmental backgrounds, which complicates our efforts to understand the disease. Genome-wide association studies (GWAS) have identified a substantial number of IBD risk loci encoding a diverse array of immune system components, many of which are shared across both subtypes of IBD and other immune-mediated diseases (1, 2). In this regard, major triggers by which patients are skewed toward either subtype of IBD lie beyond the genetic predisposition.

The gastrointestinal tract contains a vast number and a diverse array of immune cells, which together form the largest immune system in the body. Inflammatory pathways in the gut mucosa are finely controlled by the stringent mechanisms under homeostatic conditions. In the gut mucosa of IBD, excessively activated innate immune cells present antigens and secrete inflammatory cytokines, resulting in the aberrant activation of adaptive immune cells, which in turn leads to the further infiltration of inflammatory immune cells into inflamed sites and exacerbates tissue damage (3, 4). Regardless of the genetic and environmental variances of the patient cohort, dysregulated immune responses may finally converge on the common T cell–mediated inflammatory cascades, which are the direct drivers of IBD.

Despite a plethora of studies emphasizing the involvement of T cells in the pathogenesis of IBD (5, 6) and extensive efforts to develop T cell–directed strategies (7), no disease-specific T cell subset that plays an essential role in the progression of IBD has been identified. The classically proposed theory of T helper1 (Th1) and Th2 imbalance in IBD is based on the cytokine context. Given the lack of successful anticytokine therapies other than anti-Tumor necrosis factor (TNF) and anti-Interleukin (IL-12/23) antibodies (4, 8–10), detailed profiling of immune cells that goes beyond cytokines is required for future therapeutic approaches. T cells are highly plastic, which may arise from a flexible genetic program in response to local environmental cues or heterogeneity of the cells (11, 12). It is thus important to resolve how immune cell populations display pronounced diversity in the pathological settings of IBD and which of these cells contribute to pathogenesis. To address these issues, significant recent technological advances could be used to achieve breakthroughs and advance our understanding of complex biological systems. Recently,

Significance

The impact of tissue-resident memory T cells (Trm) on the pathogenesis of inflammatory bowel disease remains controversial due to their heterogeneity. In particular, the pathological function of CD4$^+$Trm, as opposed to their CD8$^+$counterparts, is largely unknown. Here, using a comprehensive analytical approach, we found that CD103$^+$CD4$^+$Trm with an inflammatory phenotype were increased in the gut of Crohn's disease (CD) patients but not in ulcerative colitis patients. Further profiling revealed that a subset of CD103$^+$CD4$^+$Trm, expressing CD161 and CCR5, were specific to CD patients and that this subset exerted cytotoxic activity. CD103$^+$CD161$^+$CCR5$^+$CD4$^+$Trm were predominant producers of proinflammatory cytokines, highlighting the importance of this specific subset in the pathogenesis of CD.

Author contributions: T.Y., M.M., and K.T. designed research; T.Y., M.M., T.K., M.A., R.K., T. Minagawa, E.O.-I., R.M., A.I., Y.S., T.A., H. Iijima, K.O., T. Mizushima, S.H., and H. Ikeuchi performed research; T.Y., M.M., S.S., M.A., J.B.W., J.N.S., D.M., D.O., and K.T. analyzed data; H. Iijima, K.O., T. Mizushima., S.H., and H. Ikeuchi co-supervised the study; and T.Y., M.M., and K.T. wrote the paper.

The authors declare no competing interest.

This article is a PNAS Direct Submission. H.O. is a guest editor invited by the Editorial Board.

[1]T.Y. and M.M. contributed equally to this work.

[2]To whom correspondence may be addressed. Email: ktakeda@ongene.med.osaka-u.ac.jp.

This article contains supporting information online at https://www.pnas.org/lookup/suppl/doi:10.1073/pnas.2204269120/-/DCSupplemental.

Published December 27, 2022.

the single-cell atlas of immune cells in IBD was reported (13–15); however, to the best of our knowledge, no comprehensive study has identified $CD4^+$ T cells differentially involved in CD and UC, and therefore, their biological properties have not been characterized.

In contrast to circulating T cells, which patrol the entire body via lymphatic and blood flow, tissue-resident T cells (Trm) remain within nonlymphoid barrier tissues and serve as the frontline of host defense, which allows for the efficient elimination of invasive pathogens (16). The contribution of Trm to the pathogenesis of IBD has been controversial, with conflicting results often being obtained in human and animal studies (17–21). This controversy is due not only to differences in patients' backgrounds but also to heterogeneity of Trm. In particular, the functional properties of $CD4^+$ Trm in pathological settings have remained largely unknown, as opposed to $CD8^+$ Trm, which have been extensively studied. Furthermore, despite the emerging importance of Trm in mouse models, it remains unclear whether animal models recapitulate the human immune responses (22). There is thus a need to analyze the functional diversity of $CD4^+$ Trm in humans and their impacts on the pathophysiology of IBD.

Here, we set out to identify T cell subsets and biological networks specifically wired in the gut in each subtype of IBD. By analyzing human gut samples, we identified the T cell subpopulations abundant in the gut in CD and UC that are differentially controlled by key transcriptional programs. Most importantly, we found that a pathogenic $CD4^+$ Trm subset with diverse properties localized adjacent to the epithelia was specifically enriched in CD and orchestrated the local inflammatory response.

Results

CD and UC Are Characterized by Distinct T Cell Subsets. To explore the specific molecular properties of each subtype of IBD, we applied mass cytometry (cytometry by time of flight: CyTOF) panels, which allow us to capture various types of T cell subsets (*SI Appendix*, Table S1). Peripheral blood mononuclear cells (PBMC) of healthy individuals and lamina propria mononuclear cells (LPMC) of the normal intestinal mucosa revealed contrasting features, highlighting the importance of profiling immune cells localized to the lesions (*SI Appendix*, Fig. S1 *A–C*). We profiled the cryopreserved intestinal LPMC isolated from the inflamed mucosa of patients with CD, UC, and unaffected mucosal regions of colon cancer patients as a control (*SI Appendix*, Table S2). Patients were subdivided into two cohort groups, with validation of the data from the first small cohort (n = 8, each group) being achieved via the second large cohort (n = 18, each group). The first cohort was randomly divided into two batches and analyzed independently to minimize the batch effect. Two-dimensional visualization of the mass cytometry data using a clustering algorithm phenograph (23) revealed T cells with distinct expression patterns of cell surface markers (Fig. 1 *A* and *B* and *SI Appendix*, Fig. S2 *A* and *B* and Table S3). Hierarchical clustering of mean marker expression revealed 19 and 16 T cell subclusters in the first and second batches, respectively. $CD3^+$ T cells of batch 1 comprised 12 $CD4^+$ and 4 $CD8^+$ T cell subclusters, with a few smaller unannotated clusters, whereas batch 2 comprised 11 $CD4^+$ and 5 $CD8^+$ T cell subclusters. Overall, CD and UC were clearly distinguished from each other by the marked changes in the specific clusters. CD patients were uniquely characterized by the massive expansion of $CD4^+$ Trm (Fig. 1 *A* and *C* and *SI Appendix*, Fig. S2*A*), which were defined by the high expression of the resident marker CD103 and the low expression of the effector memory markers CCR7 and CD27 (Fig. 1*D* and *SI Appendix*, Fig. S2*C*). In general, CD69 is also used as a marker of tissue retention (22, 24). In the gut, however, CD69 is widely expressed throughout the T cells with no cluster specificity, and 96% of CD103-expressing cells express CD69 (*SI Appendix*, Fig. S2 *D* and *E*). Thus, tissue residency in the gut was defined solely by the expression of CD103. Heat maps of the mean expression levels of T cell markers revealed that a particular fraction of $CD4^+$ Trm abundant in the gut of CD exhibited high CD161 and CCR5 compared with other T cell fractions (Fig. 1*D* and *SI Appendix*, Fig. S2*C*). The proportion of $CD45RA^-$ $CCR7^-$ $CD4^+$ effector memory T cells (Tem) was significantly higher in control than in IBD (Fig. 1 *A* and *C* and *SI Appendix*, Fig. S2*A*). In contrast, UC samples were significantly enriched in $CD45RA^+$ $CCR7^+$-naive $CD4^+$ T cells and $CXCR5^+$ $CD4^+$ T follicular helper cells (Tfh) (Fig. 1 *A*, *C*, and *D* and *SI Appendix*, Fig. S2 *A* and *C*), which is consistent with a previous report showing that Tfh increased in the gut in patients with UC (25). $CD25^{high}$ $CD127^-$ regulatory T cells (Treg) were elevated in both subtypes of IBD (*SI Appendix*, Fig. S2*F*). Meanwhile, the proportion of $CD45RA^-$ $CCR7^+$ $CD4^+$ central memory T cells (Tcm) was comparable between the groups. In contrast to the marked changes in the $CD4^+$ T cell composition, there was no pronounced change of $CD8^+$ T cells in IBD gut: The proportions of naive $CD8^+$ T cells, $CD8^+$ Tem, and γδT cells among $CD3^+$ T cells were comparable between the groups, while only a significant increase in $CD8^+$ Trm in CD compared with that in UC, but not with that in control, was observed (*SI Appendix*, Fig. S2*F*). This is partly in line with a previously reported single-cell atlas on UC gut that showed a decrease in $CD8^+$ Trm in UC (13). In contrast, the expansion of $CD8^+$ Trm in the UC gut has been shown (25). This difference may reflect the heterogeneity of $CD8^+$ Trm detected in each study. Because the involvement of $CD4^+$ Trm on CD pathogenesis has been little studied, we further characterized $CD4^+$Trm.

Analysis of the larger second cohort revealed that $CD4^+$ Trm were significantly increased in CD, confirming the first cohort data (Fig. 1*E*). We next examined whether we could deduce the cellular markers that would enable us to enrich the potentially detrimental lymphoid fraction. The results of the mean value of each marker in cohort 1 (Fig. 1*B*) were replicated by the expression marker analysis of cohort 2: $CD4^+$ Trm showed higher expression of CCR5, CD161, CD127, CD69, and CCR6 accompanied by lower expression of CCR7 and CD27 when compared with the other $CD4^+$ T cell subsets (*SI Appendix*, Fig. S3*A*). Furthermore, $CD4^+$ Trm–expressing CCR5 or CD161 produced significantly higher Interferon (IFN)-γ levels upon phorbol 12-myristate 13-acetate (PMA)/ionomycin stimulation than their counterparts that did not express these markers. Meanwhile, no differences were observed between $CD127^+$ Trm or $CCR6^+$ Trm and their respective negative counterparts (*SI Appendix*, Fig. S3*B*). On the basis of these results, we gated the $CD161^+$ $CCR5^+$ $CD4^+$ Trm, which we named "CDpop" (CD–enriched population) (Fig. 1*F*). Indeed, CDpop, but not non-CDpop Trm ($CD161^-$ or $CCR5^-$ $CD4^+$ Trm), was more abundant in CD than in UC and control (Fig. 1*E*). IFN-γ and granzyme A (GZMA) secretion induced by PMA/ionomycin was higher in CDpop than in $CD4^+$ Trm, confirming that CDpop is potentially a more activated cytotoxic subset among $CD4^+$ Trm (Fig. 1*G*). According to a previous report, the number of CD103-expressing T cells shows a gradual decline along the intestine (17). Because CD, but not UC and colon cancer, frequently affects the proximal colon rather than the distal colon, it was inevitable that our samples would be unevenly distributed along the entire colon between the groups. Nevertheless, the abundance of CDpop was significantly higher in CD than in UC and control, even when confined to the distal colon (*SI Appendix*, Fig. S3*C*), ruling out the location having an effect on our results.

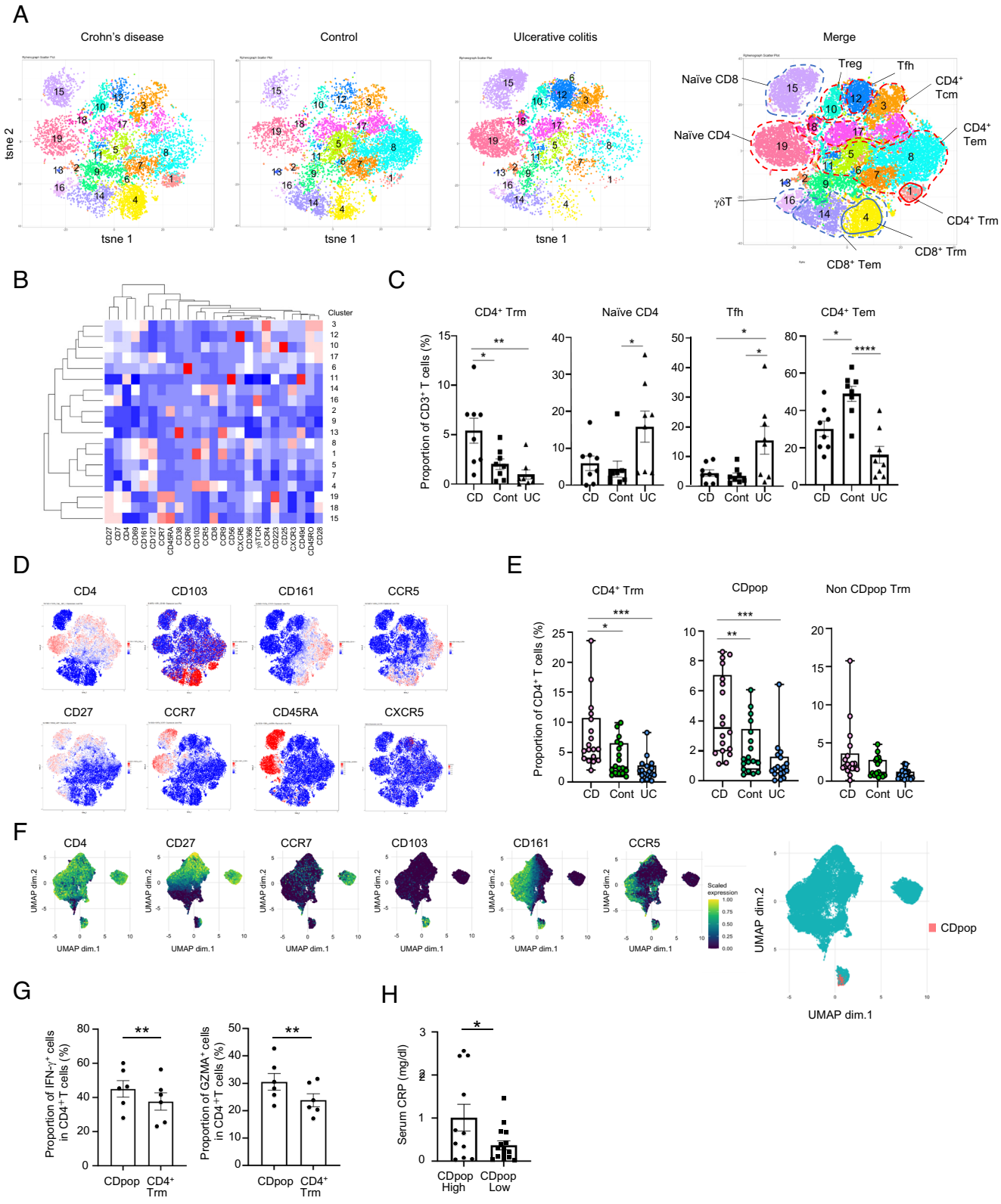

Fig. 1. Proteomic profiles of intestinal lymphocytes in IBD revealed by mass cytometry. (*A*) Phenograph-based visualization on the tSNE plot of $CD3^+$ T cells from frozen LPMC of the first batch of the first cohort of patients. Annotation of each subcluster on merged tSNE. $CD4^+$ and $CD8^+$ T cells are circled by red and blue dashed lines, respectively, and Trm by solid lines in their respective colors. Each sample (n = 4 per group) was concatenated together. (*B*) Heat map of mean expression values of T cell markers. (*C*) Cell type proportions of $CD3^+$ T cells in the first cohort of patients (n = 8 per group, batches 1 and 2). $^*P < 0.05$, $^{**}P < 0.01$, $^{****}P < 0.0001$, mean ± SEM, one-way ANOVA (Tukey's multiple comparison test). (*D*) Expression level of each cell surface marker associated with CD- and UC-predominant $CD4^+$ T cell subsets was overlaid on the tSNE plot. Representative markers high in CD- and UC-predominant T cell subsets are shown in *Upper* and *Lower* rows, respectively. (*E*) Proportions of $CD4^+$ Trm, CDpop, and the rest of $CD4^+$ Trm (non-CDpop Trm) among $CD4^+$ T cells in each sample. $^*P < 0.05$, $^{**}P < 0.01$, $^{***}P < 0.001$, n = 18 per group, one-way ANOVA (Tukey's multiple comparison test). (*F*) UMAP of the second cohort of patients (n = 18 per group). tSNE overlay of selected markers is shown. (*G*) Proportion of IFN-γ^+ and $GZMA^+$ cells in $CD4^+$ Trm and CDpop derived from CD patients after stimulation with PMA/ionomycin for 2 h. $^{**}P < 0.01$, n = 6 per group, mean ± SEM, two-tailed paired Student's *t* test. (*H*) Serum CRP levels of $CDpop^{high}$ (n = 11) and $CDpop^{low}$ (n = 15) patients before surgery. $^*P < 0.05$, mean ± SEM, two-tailed paired Student's *t* test.

Substantial expansion of CDpop was found in a subset of CD patients (Fig. 1*E*), and therefore, we stratified patients by the frequency of CDpop, with a cutoff value of 4% of $CD4^+$ T cells, which is the overall mean in frozen samples, and investigated whether it correlated with their clinical history. The medical records of CD patients showed that serum CRP levels before surgery were significantly higher in the $CDpop^{high}$ than in the $CDpop^{low}$ group (Fig. 1*H*). Further analysis using fresh colonic biopsy specimens from another cohort of CD patients revealed a positive correlation between %CDpop and International Organization for the Study of Inflammatory Bowel Diseases scores, a measure of disease activity in CD (26) (*SI Appendix*, Fig. S3*D*). Altogether, these findings suggest that an increase in local CDpop is associated with more severe disease activity of CD.

Single-Cell Transcriptional Landscape of IBD Recapitulates Mass Cytometry Results. We next performed single-cell targeted RNA-sequencing (scRNA-seq) analysis of $CD3^+$ T cells separated by fluorescence-activated cell sorting (FACS) to identify the transcriptional landscape of IBD gut. Given the predominance of specific T cells with unique cell surface marker sets in each IBD subtype, we applied the BD AbSeq system, which enables the simultaneous detection of targeted protein and mRNA (*SI Appendix*, Table S4*A*). T cells freshly isolated from the inflamed colonic mucosa of IBD patients and unaffected normal regions of the gut mucosa from colon cancer patients were analyzed (*SI Appendix*, Table S2). A total of 85,524 cells (comprising 25,171 for controls, 27,779 for CD, and 32,574 for UC) from 12 patients (n = 4 per group) were encapsulated for cDNA synthesis with the BD Rhapsody system. Following batch effect correction of the data by the Scanorama algorithm, we projected cells in two dimensions using Uniform Manifold Approximation and Projection (UMAP) (Fig. 2*A*). $CD3^+$ lymphocytes were subdivided into 17 subclusters comprising nine $CD4^+$ T cells, six $CD8^+$ T cells, CD4/CD8 double-positive cells, and a mixed subcluster of CD4 and CD8 single-positive cells; each subcluster was assigned to the major cell types by its unique transcriptional signature (Fig. 2*A* and *SI Appendix*, Figs. S4 and S5 and Table S5), and clusters were ranked in their order of abundance. First, transcriptional and translational levels of selected markers correlated well with each other, except for *ITGAE* encoding CD103 (*SI Appendix*, Fig. S6 *A* and *B*). In contrast to the highly exclusive distribution of CD103, *ITGAE* was ubiquitously expressed across the subclusters, indicating the posttranscriptional regulation of the expression of this molecule. Tem, naive T cells, and Tcm were annotated based on the combination of expression levels of CD45RA and *CCR7*: $CD45RA^-$ *CCR7*$^-$ T cells as Tem, $CD45RA^+$ *CCR7*$^+$ as naive T cells, and $CD45RA^-$ *CCR7*$^+$ as Tcm. $CD4^+$ Tem did not display discrete clusters of T helper subtypes, such as Th1 and Th2, but was rather defined by the continuous activation and effector status of each cluster, as previously described (27, 28). The largest T cell subpopulation was $CD161^{high}$ $CD4^+$ Tem (clusters 1, 5, and 6) (Fig. 2*A* and *SI Appendix*, Fig. S6*A*), which indicated its potential polarization toward Th17 lineages (29). Cluster 21 was enriched in cytotoxic genes such as *GZMs* and *NKGs*, implying the cytotoxic nature of this cluster, which was compatible with cytolytic $CD4^+$ T cells ($CD4^+$ CTL) (30) (*SI Appendix*, Figs. S4 and S5). This subset was not detected by the mass cytometry analysis, probably due to the lack of appropriate cell surface markers. Remarkably, the transcriptional landscape of CD, UC, and control displayed substantial differences between the groups, which strengthened the results of mass cytometry analysis (Fig. 2 *B* and *C*). In line with the CyTOF results (Fig. 1*C* and *SI Appendix*, Fig. S2*F*), $CD4^+$ Tem (clusters 1, 5, and 6) was predominant in control samples, while $CD4^+$ Trm (cluster 12) was elevated in CD samples. Furthermore, Tfh (cluster 8) highly expressing master transcription factor transcripts *BCL6* and *TCF7* (31–33) together with *CXCL13*, encoding a ligand for CXCR5 (34), tended to increase in UC.

CD and UC Are Transcriptionally Wired by Programs Acting in Opposing Directions. To understand the transcriptional divergence underpinning disease-specific adaptive immunity, we compared the transcriptional landscape of CD and UC $CD4^+$ lymphocytes and found that several transcription factor transcripts were differentially expressed (Fig. 2 *D* and *E*). For instance, *PRDM1* encoding B Lymphocyte-Induced Maturation Protein (BLIMP-1), which is dominantly expressed in effector T cells (35) and regulates a transcriptional program of tissue residency (36), was up-regulated in CD compared with the level in UC. In contrast, *BCL6* and *TCF7*, whose protein products are reciprocally antagonistic transcription factors of BLIMP-1 (31–33), were enriched in UC. *LEF1*, which like *TCF7* was highly expressed in both naive T cells and Tfh, contributes to the differentiation of Tfh through the regulation of *Bcl6* (32, 33).

Multiresolution Reconciled Tree (MRtree) constructs trees that effectively reflect the extent of transcriptional distinctions among cell groups and align with the levels of functional specialization (37). MRtree applied to scRNA-seq datasets revealed that the first split created two major groups: the right major branch and the left major branch (Fig. 2*F*). Importantly, $CD4^+$ Trm belonged to the right branch consisting primarily of the $CD8^+$ subsets rather than the left branch consisting of the $CD4^+$ subsets, indicating that the transcriptional signature of $CD4^+$ Trm is more closely related to that of $CD8^+$ T cells. Indeed, gene enrichment analyses of differentially expressed genes showed that the right major branch, including $CD4^+$ Trm, was enriched in the terms "natural killer cell–mediated cytotoxicity" and "granzyme-mediated programmed cell death signaling pathway," whereas genes related to the terms "regulation of alpha–beta T cell activation" and "Th17 cell differentiation" were enriched in the left major branch (*SI Appendix*, Fig. S7 *A* and *B*).

Trajectory inference methods order cells based on similarity in their gene expression patterns, which allow us to infer cell differentiation, cell activation, and the phase of cell cycle transition (38). Cell lineage and pseudotime inference analysis using Slingshot (39) by Seurat divided $CD4^+$ lymphocytes into four lineages (*SI Appendix*, Fig. S8*A*). Lineage 1 was directed to $CD4^+$ Trm, lineage 2 to $CD4^+$ Tem, lineage 3 to Tfh, and lineage 4 to $CD4^+$ CTL, among which CD, control, and UC deviated toward lineages 1, 2, and 3, respectively (*SI Appendix*, Fig. S8*B*). As such, CD and UC are transcriptionally controlled by programs acting in conflicting directions, and thus, an imbalance between two mutually opposing differentiation programs might underpin the unique phenotype of each IBD subtype.

Tissue-Resident Memory T Cells Are Reprogrammed in CD Gut to Initiate Effector and Innate Functions. We next attempted to define the transcriptional signature of a unique $CD4^+$ Trm subset, CDpop. By plotting $CD4^+$ $CD103^+$ $CD161^+$ $CCR5^+$ $CD27^-$ $CCR7^-$ cells on the UMAP (Fig. 3*A*), CDpop formed a well-defined cluster as it was almost exclusively mapped on the portion of the $CD4^+$ Trm (cluster 12) (Fig. 3*B*). Cells within the CDpop highly expressed *GZMA* and *IFNG* under unstimulated conditions (Fig. 3*C*). Genes differentially expressed between CDpop and the rest of the $CD4^+$ T cells revealed that transcripts of chemokines and *IFNG* were significantly up-regulated in CDpop, whereas genes related to a resting phenotype were up-regulated in the rest of the $CD4^+$ T cells (Fig. 3*D*). Pathway analysis of these

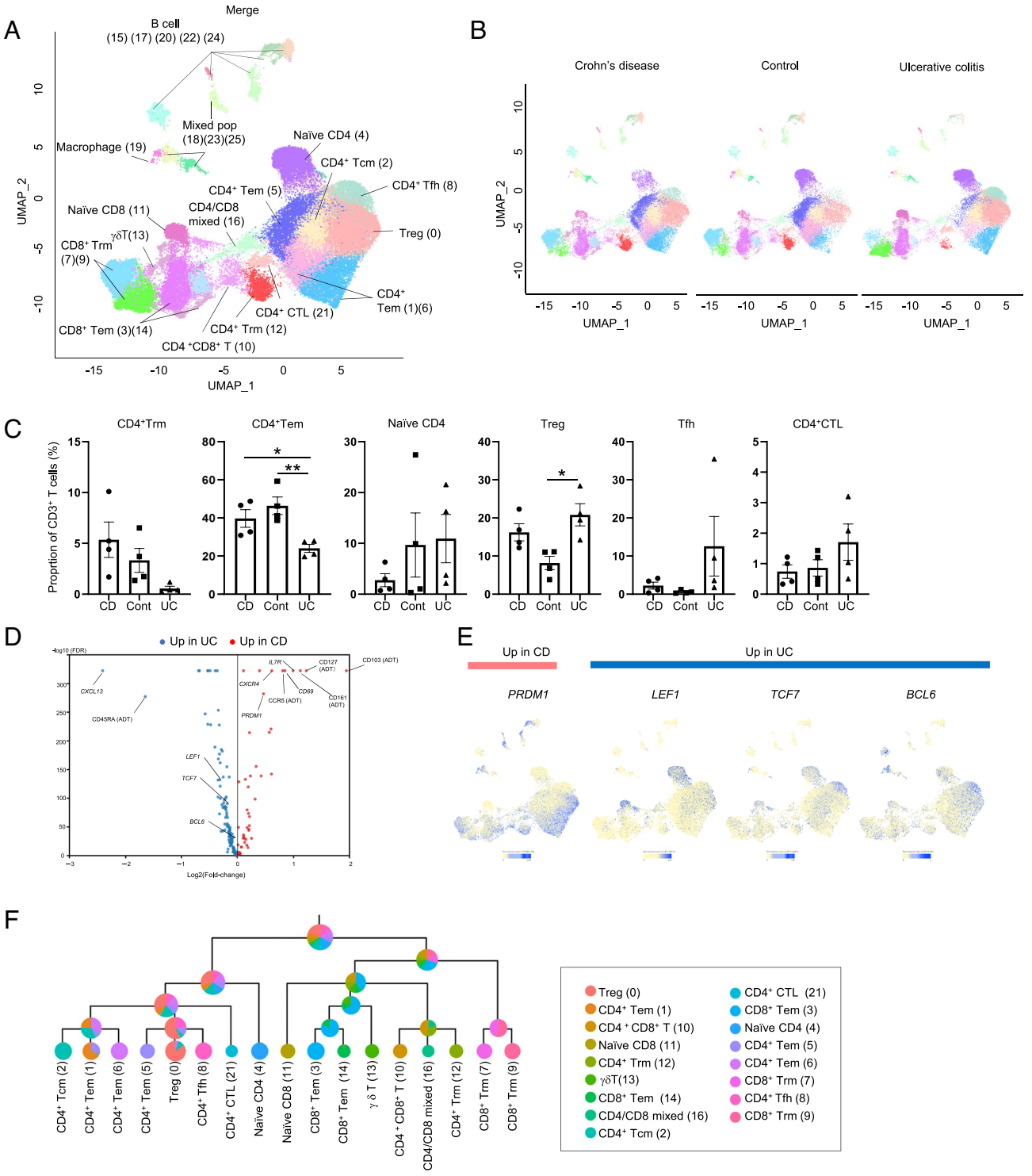

Fig. 2. Single-cell transcriptional landscape of colonic lymphocytes in IBD. (*A*) UMAP plot of FACS-sorted CD3⁺ T cells in fresh colonic samples (n = 4 per group). Cluster number is in parentheses. Data from CD, UC, and controls were merged. (*B*) UMAP plot of FACS-sorted CD3⁺ T cells in each group. (*C*) Cell type proportions of each CD4⁺ T cell subset in CD3⁺ T cells. *$P < 0.05$, **$P < 0.01$, ****$P < 0.0001$, mean ± SEM, one-way ANOVA (Tukey's multiple comparison test). (*D*) Volcano plot of genes differentially expressed between CD and UC CD4⁺ T cell subclusters. ADT: antibody-derived tag. (*E*) Gene expression plot of representative transcription factor transcripts that were significantly up-regulated in CD (*PRDM1*) or in UC (*LEF1*, *TCF7*, and *BCL6*) was overlaid on the UMAP plot. (*F*) MRtree that reveals the transcriptional distinctions and similarities between cell types. The pie charts on tree nodes represent the cell type composition in each cluster.

up-regulated genes included "IL-12 pathway" and "inflammatory response" (*SI Appendix*, Fig. S9). Together with the results of MRtree that revealed that the transcriptional signature of CD4⁺ Trm is closer to that of CD8⁺ T cells than to those of other CD4⁺ T cell subsets, these results indicate that CDpop is a colitogenic T cell subset that potentially secretes inflammatory cytokines and cytotoxic molecules in pathological settings. On the basis of these findings, we further subdivided CDpop to see if we could narrow it down into a more inflammatory CD-specific CD4⁺ Trm fraction. Indeed, reclustering of CDpop clearly demarcated CD-specific CD4⁺ Trm (CDtrm: cluster 2 in Fig. 3*E*) and the rest of the CDpop (Fig. 3 *E* and *I*). This newly emerged population in CD appeared and accumulated specifically in CD but not in control and UC (Fig. 3 *E* and *H*). CDtrm displayed the higher

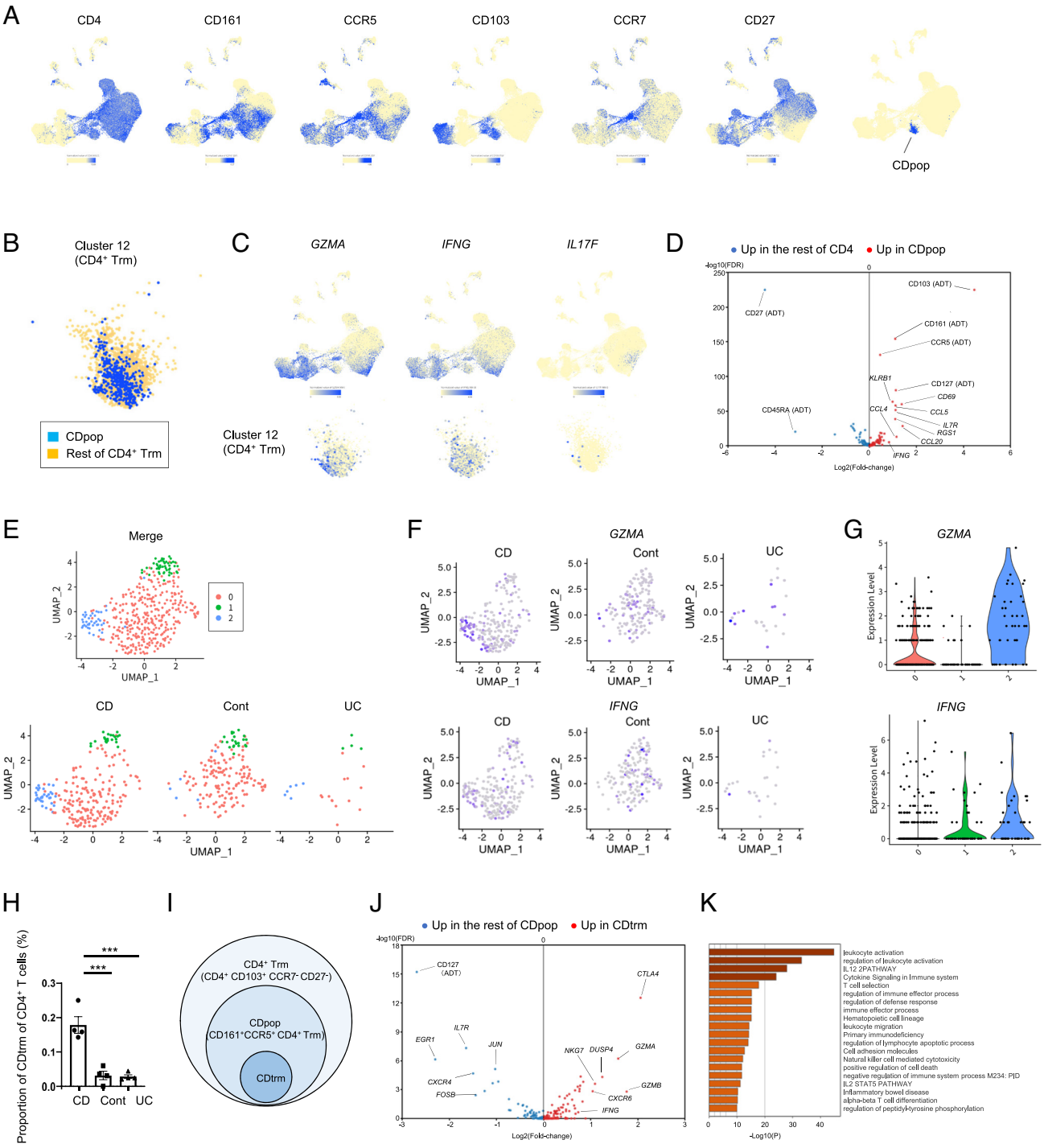

Fig. 3. Transcriptional signatures of CD-predominant CD4$^+$ Trm. (*A*) Protein expression of cell surface markers defining CDpop. (*B*) CDpop gated by the positive expression of CD4, CD103, CCR5, and CD161, and negative expression of CD27 and CCR7 was overlaid on cluster 12 of the UMAP plot. (*C*) Gene expression plot of secretory proteins overlaid on CD3$^+$ T cells (*Upper* row) and cluster 12 (*Lower* row) of the UMAP. (*D*) Volcano plot of genes differentially expressed between CDpop and the rest of the CD4$^+$ T cells. (*E*) CDpop was reclustered (upper row), and CDpop in each condition was overlaid on its UMAP (*Lower* row). (*F*) Gene expression plot of *GZMA* and *IFNG* overlaid on the UMAP. (*G*) Violin plot of *GZMA* and *IFNG* in each cluster. (*H*) Proportion of CDtrm in CD4$^+$ T cells. (*I*) Diagram showing the relationships between CD4$^+$ Trm, CDpop, and CDtrm. (*J*) Volcano plot of genes differentially expressed between CDtrm and the rest of CDpop. (*K*) Bar graph of the top 20 enriched terms across genes that were significantly up-regulated in CDtrm compared with the levels in the rest of CDpop.

expression of *GZMA* and *IFNG* than the rest of CDpop (Fig. 3 *F* and *G*). Genes differentially expressed between CDtrm and the rest of CDpop revealed that *IFNG* and a substantial number of natural cytotoxicity-related genes were up-regulated in CDtrm (Fig. 3*J*). Gene ontology and pathway analyses of the up-regulated genes revealed particular association with natural killer cell–mediated cytotoxicity and "IL-12 pathway" (Fig. 3*K*). Thus, by combining scRNA-seq datasets with the selection of appropriate surface marker sets in mass cytometry, we identified a unique CD-specific CD4$^+$ Trm with innate-like properties.

CD-Predominant T Cell Subset Secretes Inflammatory Cytokines Independent of Antigen Recognition. Transcriptional profiles revealed innate-like aspects of CDtrm, and therefore, we

hypothesized that CDtrm is poised for full activation and thus quickly acquires colitogenic properties upon stimulation. We investigated whether CDtrm is responsive to cytokine stimuli independent of T cell receptor (TCR) ligation. CDpop, which contains CDtrm and can readily be isolated by cell surface marker sets, was used for the analysis. On the basis of the transcriptional profile of CDpop that partially displays Th1 signatures, such as high *IFNG* and IL-12 signaling pathways (Fig. 3*D* and *SI Appendix*, Fig. S9), we stimulated LPMC with IL-12 and IL-18, which resulted in the release of IFN-γ from CDpop (Fig. 4*A*). Additionally, a high expression level of IL-7 receptor subunit in this cluster (*SI Appendix*, Figs. S4 and S6*A*) prompted us to stimulate cells with common gamma-chain (γc) family cytokines IL-7 and IL-15, which are necessary for intrinsic TCR tuning and sensitization (40, 41). Although homeostatic cytokines alone induced little cytokine secretion from CDpop, synergistic enhancement of IFN-γ secretion was observed by the exposure to γc cytokines in combination with IL-12 and IL-18 (Fig. 4*A*). This result was replicated in an experiment using FACS-sorted $CD3^+$ T cells to exclude the effect of other cells contained in LPMC (*SI Appendix*, Fig. S10*A*), which confirmed the validity of the direct effect of exogenous cytokines on CDtrm.

Unconventional T cells, such as mucosa-associated invariant T cells (MAIT), NK-T cells, and γδT cells, contribute to both innate and adaptive arms of the immune system and thus secrete cytokines in a TCR–independent manner (42, 43). In general, γδT cells and MAIT are relatively abundant in the gut, whereas NK-T cells are rare among the human T cell population (44). Although most of the unconventional T cells are positive for CD8, a minor portion of unconventional T cells are $CD4^+$ T cells. Indeed, 3.2% and 6.5% of LP $CD4^+$ T cells were positive for TCR Vα7.2 and γδTCR, respectively, and a portion of CDpop accounting for 7.0% and 10.4% of the total overlapped with TCR Vα7.2 and γδTCR, respectively (*SI Appendix*, Fig. S10*B*). To rule out the possible effects of unconventional T cells contained in CDpop, MAIT and γδT cells were negatively selected from CDpop, and the proportion of IFN-γ–producing cells was subsequently evaluated (Fig. 4*B*). The rate of IFN-γ^+ cells in CDpop increased after the exclusion of unconventional T cells, confirming that contaminated unconventional T cells were not the major source of IFN-γ secreted from CDpop. The proportion of IFN-γ–producing cells among CDpop was significantly higher than that of the entire $CD4^+$ T cells (Fig. 4*C*), emphasizing the cytokine-sensitive properties of this specific subset.

We next examined whether CDpop with negative selection of unconventional T cells was differentially responsive to TCR and cytokine stimulation. TCR stimulation by anti-CD3/CD28 antibodies resulted in the pan activation of $CD4^+$ T cells, and TCR stimulation alone showed IFN-γ production in CDpop comparable to that in the entire $CD4^+$ T cells (Fig. 4*D*). Indeed, the cytokine/TCR response ratio for IFN-γ secretion in each sample was significantly higher in CDpop than in $CD4^+$ T cells, reflecting the cytokine-sensitive nature of CDtrm (Fig. 4*E*). Thus, the secretion of IFN-γ from CDpop was specifically and maximally enhanced by cytokine stimulation. Secretion of tumor necrosis factor-α (TNF-α, another Th1 cytokine) was significantly lower in CDpop than in total $CD4^+$ T cells stimulated with TCR (Fig. 4*F*). These findings indicate that CDtrm possesses innate cell-like properties in addition to Th1 properties.

CD-Predominant T Cell Subset Is the Main Source of TCR-Independent IFN-γ Production. To gain broader insight into cytokine-responding T cells, we performed mass cytometry analysis in frozen LPMC stimulated by a cytokine cocktail. Seven probes against intracellular cytokines were added to the previous surface marker antibody panel (*SI Appendix*, Table S6). Samples were stimulated overnight with or without cytokines. Cell surface markers were used for the clustering process, and the cytokine plot was subsequently overlaid on the map. A phenograph revealed that a mixed population of stimulated and unstimulated $CD4^+$ T cells was subdivided into 17 subclusters, some of which responded well to the cytokine cocktail, as shown by the upregulation of CD25 and CD28 accompanied by the downregulation of CD127 after stimulation (Fig. 4*G*). As observed in the previous flow cytometry analysis (Fig. 4*A*), cytokine cocktail stimuli drove CDpop, corresponding to a portion of cluster 5 (Fig. 4 *G* and *H*), to secrete high levels of IFN-γ and IL-2 (Fig. 4 *I* and *J*). A heat map of mean marker expression revealed that cluster 16 is $CD161^+$ $CD4^+$ Tem, which were distinguished from CDpop by the negative expression of CD103. This subset was predominant in controls in CyTOF analysis (Fig. 1 *A* and *B* and *SI Appendix*, Fig. S2 *A* and *B*) and secreted only a small amount of IFN-γ (Fig. 4 *I* and *J*). In contrast, TNF-α, IL-17, and IL-4 production did not differ between the subsets. These findings were reproduced in the same experiments with fresh samples, ruling out the possibility that the freezing and thawing process itself stimulates cells to secrete inflammatory cytokines (*SI Appendix*, Fig. S10*C*). Because the cytokine cocktail is more potent at stimulating type 1 cytokine secretion, we next examined the cytokine-producing potential of CDpop by applying stimulation with PMA/ionomycin to further examine potential cytokine production. Similar to the effects of the cytokine cocktail, PMA/ionomycin also induced significantly higher levels of IFN-γ and IL-2 secretion from CDpop compared with the levels in other $CD4^+$ T cell fractions (*SI Appendix*, Fig. S10*D*). Additionally, GZMA was significantly higher in CDpop than in other $CD4^+$ fractions in both unstimulated and stimulated conditions, which is in line with the scRNA-seq results. IL-17 and TNF-α, which were not secreted in response to cytokine cocktail stimuli, were induced by PMA/ionomycin treatment and were significantly elevated in CDpop compared with the levels in other $CD4^+$ fractions, implying the pleiotropic nature of CDpop with innate and Th1/Th17 signatures. Thus, in the cytokine milieu of IBD, CDpop may produce proinflammatory cytokines continuously even in the absence of specific antigen stimulation, which may in turn contribute to the persistence of chronic inflammation.

Restricted Clonality of CD-Predominant T Cells Is Observed in a Portion of CD Patients. To elucidate the clonality of expanded CDpop, we next performed TCR-seq on FACS-sorted CDpop from 6 $CDpop^{high}$ patients. The mean percentage of CDpop in $CD4^+$ T cells of the subjects was 7.1 ± 1.8%, which was higher than the cutoff value of 4% of frozen $CD4^+$ T cells. Overall, the clonal structure of CDpop from CD patients was highly diverse and polyclonal, and only a limited number of clones were shared between the patients (*SI Appendix*, Fig. S11*A* and Table S7). The clonotypes in each patient used a broad spectrum of TCR Vα and Vβ genes (*SI Appendix*, Fig. S11*B*). In patient 1, the specific clonotype 1 and the top 10 clonotypes accounted for 11% and 35% of the total, respectively. Meanwhile, even the highest ranked clones in patients 2 to 6 accounted for 0.9 to 3.4%. We finally assessed the antigen specificity of the top 10 $CD4^+$ T cell clonotypes in each patient by referring to the McPAS-TCR database (45). Although none of the CDR3 sequences matched perfectly to known pathogen- or immune disease-associated sequences, the clonotype 1 sequence was analogous to that of previously reported IBD-associated clonotype (46), with two amino acid substitutions. As such, polyclonal proliferation underlies the expansion of CDpop in CD patients, but restricted clonality of CDpop was observed in a portion of patients.

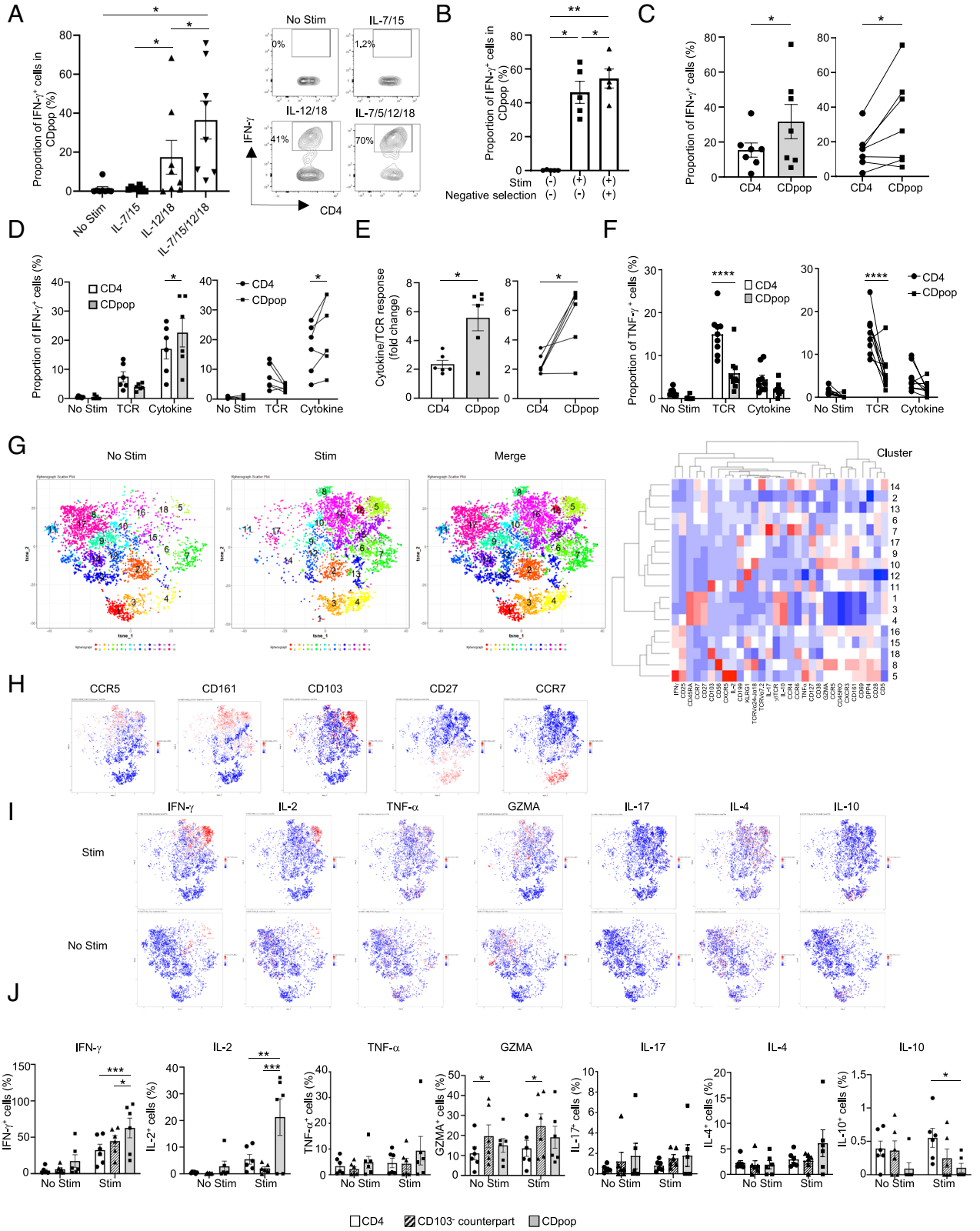

Fig. 4. Responsiveness of CD-predominant CD4$^+$ Trm to cytokines. (*A*) *Left*: Proportion of IFN-γ$^+$ cells in CDpop under cytokine stimulation in CD samples. *$P < 0.05$, n = 8 per group, mean ± SEM, two-way RM ANOVA (Tukey's multiple comparison test). *Right*: Representative images of flow cytometry analysis. (*B*) Proportions of IFN-γ$^+$ cells with or without stimulation in CDpop and CDpop with negative selection of MAIT (TCRVα7.2$^+$) and γδT cells. *$P < 0.05$ and **$P < 0.01$, n = 5 per group, mean ± SEM, RM one-way ANOVA (Tukey's multiple comparison test). (*C*) *Left*: Proportions of IFN-γ$^+$ cells in CDpop and CD4$^+$ T cells after cytokine stimulation. *Right*: The corresponding samples are connected with a line. *$P < 0.05$, n = 7 per group, mean ± SEM, two-tailed paired Student's *t* test. (*D*) *Left*: Proportions of IFN-γ$^+$ cells in CDpop and CD4$^+$ T cells after TCR or cytokine cocktail. *Right*: The corresponding samples are connected with a line. *$P < 0.05$, n = 6 per group, mean ± SEM, two-way RM ANOVA (Sidak's multiple comparison test). (*E*) *Left*: Cytokine/TCR ratio for IFN-γ secretion of each sample. *Right*: The corresponding samples are connected with a line. *$P < 0.05$, n = 6 per group, mean ± SEM, two-tailed paired Student's *t* test. (*F*) *Left*: Proportions of TNF-γ$^+$ cells in CDpop and CD4$^+$ T cells after TCR or cytokine stimulation. *Right*: The corresponding samples are connected with a line. *$P < 0.05$, n = 6 per group, mean ± SEM, two-way RM ANOVA (Sidak's multiple comparison test). (*G*) Phenograph-based visualization on the tSNE plot of frozen colonic CD4$^+$ T cells from LPMC from four CD patients and two

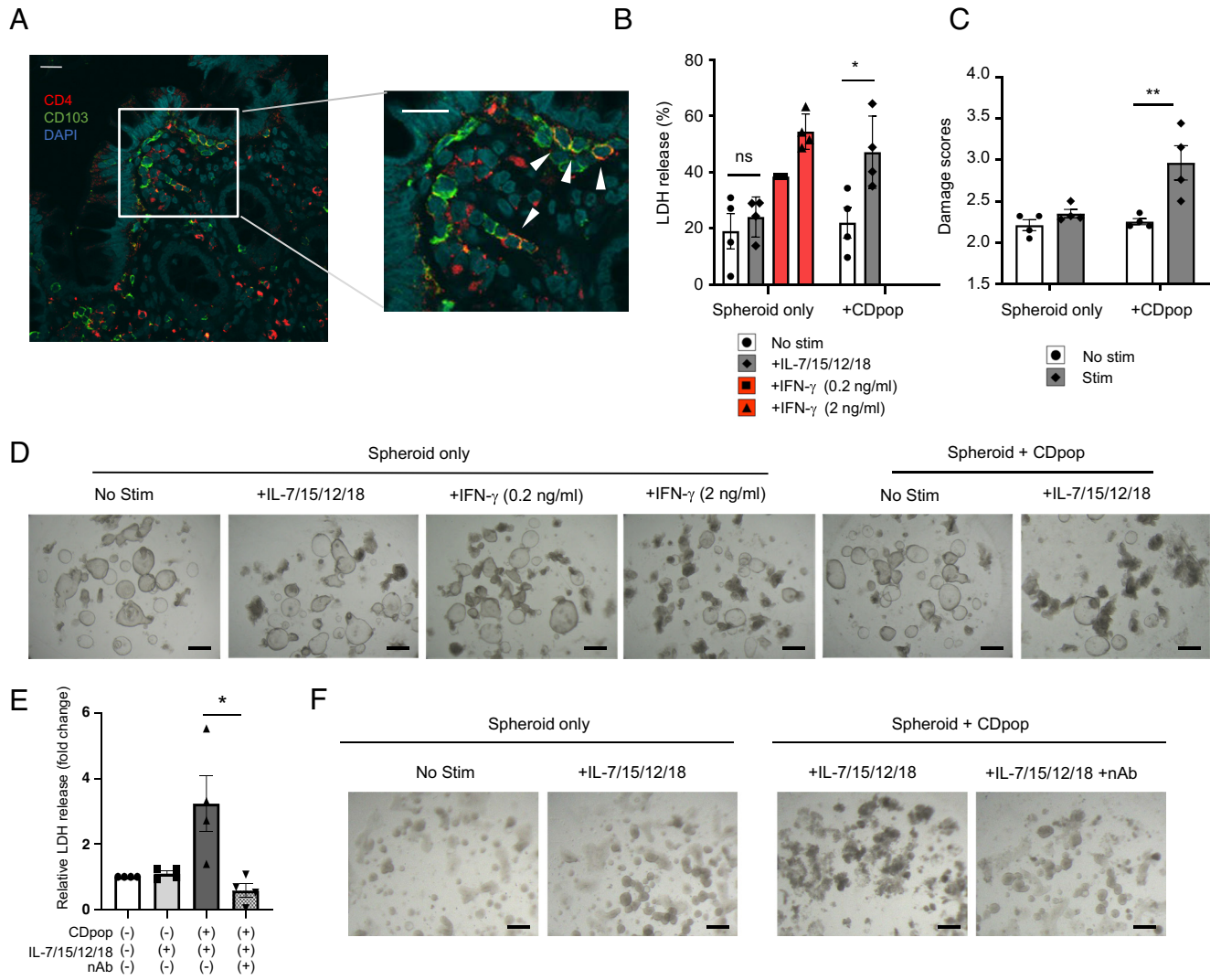

Fig. 5. Cytotoxic effect of CD-predominant CD4$^+$ Trm on epithelia. (*A*) Representative images of immunohistochemistry of LP from CD patients. (Scale bar, 20 μm.) Red, CD4; green, CD103; and blue, DAPI. White arrows show CD4$^+$ CD103$^+$ Trm in LP. (*B*) Percentage of LDH release in the culture supernatant. *P < 0.05, n = 4 per group, mean ± SEM. shown, two-way ANOVA (Sidak's multiple comparison test). (*C*) Average spheroid damage scores of four independent experiments. *P < 0.05, n = 4 per group, mean ± SEM. shown, two-way ANOVA (Sidak's multiple comparison test). (*D*) Representative images of spheroids cocultured with or without CDpop under the cytokine stimuli. (Scale bar, 200 μm.) (*E*) The effect of IFN-γ neutralizing antibody (nAb) on cytokine-stimulated CDpop evaluated by relative LDH release in the culture supernatant. *P < 0.05, n = 4 per group, mean ± SEM. shown, Dunn's multiple comparison test. (*F*) Representative images of spheroids cocultured with or without CDpop and nAb. (Scale bar, 150 μm.)

Cytotoxic Effect of CD-Predominant T Cells on the Epithelial Layer Is Maximized by Their Localization Properties. The spatial properties of cells can elicit cellular functions, and therefore, we next investigated the pathological relevance of CDpop localization in LP. Immunohistochemical evaluation of CD4 and CD103 double-positive cells including CDpop in LP revealed that they localized adjacent to the epithelia along with other CD103-expressing cells (Fig. 5*A*). In accordance with this unique spatial distribution of CD4$^+$ Trm in LP, we investigated whether CDpop can directly damage the gut epithelial layer upon stimulation. IFN-γ treatment alone injured the human gut spheroids in a dose-dependent manner (Fig. 5*B*). Notably, coculture of human-derived spheroids with FACS-sorted CDpop gated by CD4$^+$ CD103$^+$ CD161$^+$ CCR5$^+$ CD27$^-$ CCR7$^-$, stimulated with a cytokine cocktail for 72 h, resulted in epithelial damage accompanied by the elevation of Lactate Dehydrogenase (LDH) levels in the culture supernatant that is comparable to the findings observed when IFN-γ was added to the spheroids (Fig. 5 *B*–*D*). In contrast, coculture with CDpop without cytokine cocktail did not disrupt the spheroid structure or induce LDH release. Furthermore, IFN-γ neutralizing antibody canceled the effect of cytokine-stimulated CDpop on the gut spheroids (Fig. 4 *E* and *F*). Thus, IFN-γ produced by CDpop exerts its colitogenic effects by directly damaging the adjacent epithelial barrier. Together with the previous findings that IL-12, IL-15, and IL-18 are

controls (n = 6 per condition and n = 12 merged) stimulated with or without cytokine cocktail. Heat map of mean expression values of T cell markers is shown on the right. (*H*) tSNE overlay of selected surface marker expression on merged plot. (*I*) tSNE overlay of cytokine markers in stimulated and unstimulated samples. (*J*) Proportion of each cytokine-positive cell in total CD4$^+$ T cells, CD103$^-$ counterpart of CDpop, and CDpop after stimulation by cytokine cocktail. ***P < 0.05, **P < 0.01, ***P < 0.001, n = 6 per group, mean ± SEM, two-way RM ANOVA (Sidak's multiple comparison test).

highly expressed in the affected LP of IBD (47–49), these observations support the notion that CDpop can be maximally enhanced both by the unique cytokine milieu in IBD gut and by the localization site in vivo.

Discussion

Using single-cell technologies on LPMC derived from human samples, we identified a $CD4^+$ Trm subset that was specifically increased in CD. This CD-specific T cell subset, reprogrammed into effector and innate-like phenotypes, is capable of directly damaging adjacent epithelial cells, thereby exerting a pathogenic effect. Trm is characterized by the expression of C-type lectin-like molecules CD69 and CD103, which are the αE subunits of αEβ7 integrin involved in the adhesion of lymphocytes to epithelial cells. Although $CD69^+$ T cells have been reported to exhibit tissue-localized properties, $CD103^+$ T cells were specifically referred to as Trm in this study because the majority of lymphocytes express CD69 in the gut (24, 50). The present study showed that the expression of CD103 is mainly regulated at the posttranscriptional level. Therefore, deep profiling of Trm is possible only by combining scRNA-seq analysis with protein analysis, which allowed us to identify disease-specific $CD4^+$ T cells. By taking full advantage of mass cytometry and scRNA-seq analysis, we successfully narrowed down $CD4^+$ Trm to CDtrm, and this specific subset indeed expanded drastically in CD patients.

Whether Trm plays a central role in the pathology of IBD is controversial (17–19), probably due to the difference in methodologies used in each study, high variance of the patient cohort, and the heterogeneity of Trm at the molecular level. Furthermore, most of these previous studies focused on $CD8^+$ Trm, and little is known about the pathological properties of $CD4^+$ Trm in IBD, especially in humans. The lack of appropriate cell surface markers that define CDtrm with high purity led us to perform biological validation using CDpop. Future studies may establish a more sophisticated set of markers for CDtrm, which could allow us to extend our study to future therapeutic strategies. Dissecting the diversity of $CD4^+$ Trm and targeting the inflammatory $CD4^+$ Trm fraction will further enhance the effectiveness and minimize the side effects of therapeutic interventions targeting the β7 integrin for IBD, which is already in phase III clinical trials (51).

In mice, colitogenic effects of Trm are attributed to the transcriptional regulators of Trm development (18). In addition to the regulatory function on tissue homing, BLIMP-1 encoded by *Prdm1* is responsible for the acquisition of innate-like activity by T helper cells in response to the γc cytokine IL-2 (52). Thus, the functional dichotomy of the key transcription factor may control tissue residency and innate-like activities in CDtrm. Although many studies have reported on animal models of enteritis, the findings cannot be applied directly to human pathology because the expression of molecules is not completely conserved across species, and there are no appropriate animal models that exactly reflect each subtype of IBD.

Another important aspect is that CDtrm is poised for rapid execution of effector functions by cytokine stimulation without TCR ligation. IL-12 and IL-18 synergistically induce IFN-γ production from T cells via the upregulation of *IL18R* and transcriptional enhancement of *IFNG* by transcription factors induced by both signaling pathways (53, 54). Intriguingly, we found that the synergistic effect of γc cytokines further reinforced the effector function of these cells. Indeed, increased levels of IL-12, IL-15, and IL-18 have been observed in the LP of IBD gut in previous studies (47–49). Given the proximity of Trm to epithelia, it is reasonable that $CD4^+$ Trm responds to IL-15, which can be secreted by the epithelia in concert with other inflammatory cytokines abundant in the LP of CD patients, resulting in epithelial cytotoxicity.

GWAS revealed that CD- or IBD-associated loci contain genes that encode IFN-γ and its receptor (1), highlighting the importance of IFN-γ in disease pathogenesis. Indeed, IFN-γ has been shown to be increased in the LP of CD patients (55, 56) and is required for inducing inflammation in colitis models (57, 58). IFN-γ regulates intestinal epithelial homeostasis (59, 60) and drives IBD pathogenesis through vascular barrier disruption (61, 62). Despite this plethora of findings indicating that IFN-γ is profoundly involved in intestinal inflammation, its specific neutralizing antibody fontolizumab has had limited efficacy in clinical trials (10), suggesting that additional factors are required for disease development. Intriguingly, IFN-γ, in synergy with TNF-α, promotes the apoptosis of intestinal epithelia (59). This is noteworthy because a neutralizing antibody specific for TNF-α resulted in remarkable clinical improvement (63), in contrast to the poor clinical efficacy of many other anticytokine antibodies (4, 8, 9). Furthermore, Th17 cells, which have recently received attention as the core of IBD pathogenesis, have considerably high plasticity (64, 65). In this context, the increased rate of IFN-γ–producing Th17 cells within CDpop upon PMA/ionomycin stimulation and high expression of CD161 in CDpop indicate that IFN-γ produced by CDpop may be a marker of pathogenic Th17 cells. Taking these findings together, the properties of CDtrm, that is, IFN-γ secretion and spatial proximity to the gut epithelia, should be related to susceptibility to mucosal injury.

CD and UC display distinct patterns of immune networks, which are transcriptionally wired by the programs acting in opposing directions. In contrast to the accumulation of $CD4^+$ Trm in CD, $TCF7^{high}$ Tfh were increased in a proportion of UC patients. The *TCF7* product TCF-1 induces GATA3 expression required for Th2 differentiation while blocking IFN-γ–producing Th1 cell fate (66); thus, differential *TCF7* expression may reflect the classically proposed Th1–Th2 deviation as a mechanism of IBD. This finding points to the different inflammatory gut environments that tilt the balance between these T cell lineages.

In previous studies in which single-cell analysis of immune cells in IBD was conducted, Trm expressing high levels of Th1/Th17-related cytokines (14) and intraepithelial Th17 cells (67) were described. However, the functional role and pathological relevance of these cells have not yet been explored. Furthermore, most previous studies focused on one of the two subtypes of IBD, preventing a disease-specific program of T cell differentiation from being revealed. By the comprehensive analysis of human samples, we showed that distinct immune networks were rewired in each IBD subtype. In CD, gut-resident T cells were expanded. This included a subset of $CD4^+$ Trm, which we identified to be the most pathogenic and poised to exert effector and cytotoxic responses upon inflammatory stimuli. In contrast, the shift toward the Tfh differentiation program in a proportion of UC patients is possibly associated with the increased pathological IgG^+ plasma cells in the UC setting (25, 68) and basal plasmacytosis observed in UC histology (69). In summary, our findings shed light on the transcriptional and proteomic landscape of adaptive immunity in IBD, highlighting the potential roles of a specific T cell subset in the pathogenesis of this disease.

Materials and Methods

Detailed methods are available in *SI Appendix*, Methods.

LPMC Isolation. The normal intestinal mucosa was obtained from macroscopically intact areas in patients with colorectal cancer. The inflamed intestinal mucosa was obtained from surgically resected specimens from patients with IBD. Briefly, intestinal epithelial cells were dissociated by shaking in 5 mM

ethylenediaminetetraacetic acid (EDTA) in Hanks' Balanced Salt Solution, followed by removal of the muscle layer. The mucosal layer was cut into pieces and digested with 1 mg/mL collagenase type 1 (Sigma Aldrich) mixed with 0.07 IU/mL DNase in RPMI 1640 for 30 min at 37 °C. Cells were centrifuged at 800 g, dispersed in EDTA solution, and washed in phosphate-buffered saline (PBS). LPMC were frozen in liquid nitrogen until analysis. The same procedure was followed for cell isolation from biopsy samples, except that removal of the muscle layer was not required.

Mass Cytometry. Cryopreserved LPMC and PBMC were barcoded with a combination of anti-CD45 antibodies (89Y, 115In, and 175Lu) for 30 min at RT and washed with Maxpar Cell Staining Buffer (Fluidigm). After centrifugation, cells were stained with an antibody mix (*SI Appendix*, Tables S1 and S5) for 45 min at RT. After washes, cells were incubated with cisplatin (1:1,000, Cell-ID™ Cisplatin-^{198}Pt; Fluidigm) for 5 min at RT, quenched with Maxpar Cell Staining Buffer, and fixed with 2% PFA for 30 min at 4 °C. For intracellular staining, eBioScience Fix/Perm Buffer (Invitrogen) was added to cells and centrifuged, stained with markers dissolved in Fix/Perm Buffer for 45 min at 4 °C, and washed with Fix/Perm Buffer. After centrifugation, the pellet was incubated with iridium (1:1,000, Cell-ID™ Intracalator-Ir; Fluidigm) overnight at 4 °C, washed, and acquired on CyTOF Helios (Fluidigm). EQ beads were used for normalization.

Single-Cell RNA-Seq and BD AbSeq. LPMC were freshly prepared from surgically resected samples and stained with FITC anti-human CD3 antibody (clone HIT3a; BioLegend) for 30 min at 4 °C, followed by dead cell staining, after which cells were sorted on a Becton, Dickinson and Company (BD) FACSAria. Sorted live CD3$^+$ cells were incubated with BD AbSeq antibodies (BD Biosciences) conjugated with oligonucleotides (*SI Appendix*, Table S4) for 30 min at 4 °C and washed in PBS. Subsequently, a single-cell suspension was loaded onto BD Rhapsody (BD Biosciences), followed by the loading of a bead library onto the cartridge. The cells were lysed to hybridize mRNAs onto barcoded capture oligos on the beads. The beads were collected into a single tube for the subsequent steps of complementary DNA (cDNA) synthesis, exonuclease I digestion, and multiplex PCR-based library construction. The BD Rhapsody Immune Response Panel for human and a custom primer set (*SI Appendix*, Table S4) were used for library generation. Libraries were sequenced on the Illumina HiSeq 3000 platform (2 × 100 bp).

Data, Materials, and Software Availability. Single-cell RNA data are available on website with the accession number GSE218000: https://www.ncbi.nlm.nih.gov/geo/query/acc.cgi?acc=GSE218000. All other data are included in the article and/or *SI Appendix*.

ACKNOWLEDGMENTS. This work was supported by Grants-in-Aid for Scientific Research (18K15812 to M.M. and 18H04028 to K.T.) and the Japan Agency for Medical Research and Development (20gm101004 to K.T.). We thank all of the patients and medical staff at the Osaka University and Hyogo College of Medicine who contributed to this study. We are also grateful to Masaharu Kohara and Yui Magota for technical assistance and Chisa Hidaka and Miki Yamaguchi for administrative assistance. We also thank all members of the Takeda laboratory for the useful comments to improve this study.

Author affiliations: [a]Department of Microbiology and Immunology, Graduate School of Medicine, Osaka University, Osaka 565-0871, Japan; [b]Immunology Frontier Research Center, Osaka University, Osaka 565-0871, Japan; [c]Department of Pediatrics, Graduate School of Medicine, Osaka University, Osaka 565-0871, Japan; [d]Department of Surgical Pathology, Hyogo College of Medicine, Hyogo 663-8501, Japan; [e]Department of Bioinformatic Engineering, Graduate School of Information Science and Technology, Osaka University, Osaka 565-0871, Japan; [f]Center for Infectious Disease Education and Research, Osaka University, Osaka 565-0871, Japan; [g]Department of Inflammatory Bowel Disease, Division of Surgery, Hyogo College of Medicine, Hyogo 663-8501, Japan; [h]Genome Information Research Center, Research Institute for Microbial Diseases, Osaka University, Osaka 565-0871, Japan; [i]Integrated Frontier Research for Medical Science Division, Institute for Open and Transdisciplinary Research Initiatives, Osaka University, Osaka 565-0871, Japan; [j]Department of Gastroenterological Surgery, Graduate School of Medicine, Osaka University, Osaka 565-0871, Japan; [k]Department of Gastroenterology and Hepatology, Graduate School of Medicine, Osaka University, Osaka 565-0871, Japan; [l]Department of Gastroenterology, Osaka Police Hospital, Osaka 543-8922, Japan; and [m]Department of Gastroenterological Surgery, Osaka Police Hospital, Osaka 543-8922, Japan

1. L. Jostins *et al.*, Host-microbe interactions have shaped the genetic architecture of inflammatory bowel disease. *Nature* **491**, 119–124 (2012).
2. J. Z. Liu *et al.*, Association analyses identify 38 susceptibility loci for inflammatory bowel disease and highlight shared genetic risk across populations. *Nat. Genet* **47**, 979–986 (2015).
3. K. J. Maloy, F. Powrie, Intestinal homeostasis and its breakdown in inflammatory bowel disease. *Nature* **474**, 298–306 (2011).
4. M. F. Neurath, Cytokines in inflammatory bowel disease. *Nat. Rev. Immunol.* **14**, 329–342 (2014).
5. C. L. Maynard, C. T. Weaver, Intestinal effector T cells in health and disease. *Immunity* **31**, 389–400 (2009).
6. T. Imam, S. Park, M. H. Kaplan, M. R. Olson, Effector T helper cell subsets in inflammatory bowel diseases. *Front Immunol.* **9**, 1212 (2018).
7. S. Paramsothy, A. K. Rosenstein, S. Mehandru, J. F. Colombel, The current state of the art for biological therapies and new small molecules in inflammatory bowel disease. *Mucosal Immunol.* **11**, 1558–1570 (2018).
8. S. R. Targan *et al.*, A randomized, double-blind, placebo-controlled phase 2 study of Brodalumab in patients with moderate-to-severe Crohn's disease. *Am. J. Gastroenterol.* **111**, 1599–1607 (2016).
9. E. Musch *et al.*, Interferon-beta-1a for the treatment of steroid-refractory ulcerative colitis: A randomized, double-blind, placebo-controlled trial. *Clin. Gastroenterol. Hepatol.* **3**, 581–586 (2005).
10. W. Reinisch *et al.*, Fontolizumab in moderate to severe Crohn's disease: A phase 2, randomized, double-blind, placebo-controlled, multiple-dose study. *Inflamm Bowel Dis.* **16**, 233–242 (2010).
11. K. M. Murphy, B. Stockinger, Effector T cell plasticity: Flexibility in the face of changing circumstances. *Nat. Immunol.* **11**, 674–680 (2010).
12. M. DuPage, J. A. Bluestone, Harnessing the plasticity of CD4(+) T cells to treat immune-mediated disease. *Nat. Rev. Immunol.* **16**, 149–163 (2016).
13. D. Corridoni *et al.*, Single-cell atlas of colonic CD8(+) T cells in ulcerative colitis. *Nat. Med.* **26**, 1480–1490 (2020).
14. J. C. Martin *et al.*, Single-cell analysis of Crohn's disease lesions identifies a pathogenic cellular module associated with resistance to anti-TNF therapy. *Cell* **178**, 1493–1508.e1420 (2019).
15. V. Mitsialis *et al.*, Single-cell analyses of colon and blood reveal distinct immune cell signatures of ulcerative colitis and Crohn's disease. *Gastroenterology* **159**, 591–608.e510 (2020).
16. D. Masopust, V. Vezys, A. L. Marzo, L. Lefrancois, Preferential localization of effector memory cells in nonlymphoid tissue. *Science* **291**, 2413–2417 (2001).
17. C. Smids, C. S. Horjus Talabur Horje, F. van Wijk, E. G. van Lochem, The complexity of alpha E beta 7 Blockade in inflammatory bowel diseases. *J. Crohns Colitis* **11**, 500–508 (2017).
18. S. Zundler *et al.*, Hobit- and Blimp-1-driven CD4(+) tissue-resident memory T cells control chronic intestinal inflammation. *Nat. Immunol.* **20**, 288–300 (2019).
19. B. Roosenboom *et al.*, Intestinal CD103+CD4+ and CD103+CD8+ T-cell subsets in the Gut of inflammatory bowel disease patients at diagnosis and during follow-up. *Inflamm. Bowel Dis.* **25**, 1497–1509 (2019).
20. H. Bottois *et al.*, KLRG1 and CD103 expressions define distinct intestinal tissue-resident memory CD8 T cell subsets modulated in Crohn's disease. *Front Immunol.* **11**, 896 (2020).
21. S. Bishu *et al.*, CD4+ tissue-resident memory T cells expand and are a major source of mucosal tumour necrosis factor alpha in active Crohn's disease. *J. Crohns Colitis* **13**, 905–915 (2019).
22. P. A. Szabo, M. Miron, D. L. Farber, Location, location, location: Tissue resident memory T cells in mice and humans. *Sci. Immunol.* **4**, 9673 (2019).
23. J. H. Levine *et al.*, Data-driven phenotypic dissection of AML reveals progenitor-like cells that correlate with prognosis. *Cell* **162**, 184–197 (2015).
24. B. V. Kumar *et al.*, Human tissue-resident memory T cells are defined by core transcriptional and functional signatures in lymphoid and mucosal sites. *Cell Rep.* **20**, 2921–2934 (2017).
25. B. S. Boland *et al.*, Heterogeneity and clonal relationships of adaptive immune cells in ulcerative colitis revealed by single-cell analyses. *Sci. Immunol.* **5**, eabb4432 (2020).
26. J. Myren *et al.*, Multinational inflammatory bowel disease survey 1976–1982. A further report on 2,657 cases. *Scand J. Gastroenterol Suppl.* **95**, 1–27 (1984).
27. E. Cano-Gamez *et al.*, Single-cell transcriptomics identifies an effectorness gradient shaping the response of CD4(+) T cells to cytokines. *Nat. Commun.* **11**, 1801 (2020).
28. E. Kiner *et al.*, Gut CD4(+) T cell phenotypes are a continuum molded by microbes, not by TH archetypes. *Nat. Immunol.* **22**, 216–228 (2021).
29. M. A. Kleinschek *et al.*, Circulating and gut-resident human Th17 cells express CD161 and promote intestinal inflammation. *J. Exp. Med.* **206**, 525–534 (2009).
30. H. Cheroutre, M. M. Husain, CD4 CTL: Living up to the challenge. *Semin Immunol.* **25**, 273–281 (2013).
31. R. J. Johnston *et al.*, Bcl6 and Blimp-1 are reciprocal and antagonistic regulators of T follicular helper cell differentiation. *Science* **325**, 1006–1010 (2009).
32. L. Xu *et al.*, The transcription factor TCF-1 initiates the differentiation of T(FH) cells during acute viral infection. *Nat. Immunol.* **16**, 991–999 (2015).
33. Y. S. Choi *et al.*, LEF-1 and TCF-1 orchestrate T(FH) differentiation by regulating differentiation circuits upstream of the transcriptional repressor Bcl6. *Nat. Immunol.* **16**, 980–990 (2015).
34. C. G. Vinuesa, S. G. Tangye, B. Moser, C. R. Mackay, Follicular B helper T cells in antibody responses and autoimmunity. *Nat. Rev. Immunol.* **5**, 853–865 (2005).
35. G. A. Martins *et al.*, Transcriptional repressor Blimp-1 regulates T cell homeostasis and function. *Nat. Immunol.* **7**, 457–465 (2006).
36. L. K. Mackay *et al.*, Hobit and Blimp1 instruct a universal transcriptional program of tissue residency in lymphocytes. *Science* **352**, 459–463 (2016).
37. M. Peng *et al.*, Cell type hierarchy reconstruction via reconciliation of multi-resolution cluster tree. *Nucleic Acids Res.* **49**, e91 (2021).
38. W. Saelens, R. Cannoodt, H. Todorov, Y. Saeys, A comparison of single-cell trajectory inference methods. *Nat. Biotechnol.* **37**, 547–554 (2019).
39. K. Street *et al.*, Slingshot: Cell lineage and pseudotime inference for single-cell transcriptomics. *BMC Genomics* **19**, 477 (2018).
40. J. Sprent, C. D. Surh, Normal T cell homeostasis: The conversion of naive cells into memory-phenotype cells. *Nat. Immunol.* **12**, 478–484 (2011).
41. P. Deshpande *et al.*, IL-7- and IL-15-mediated TCR sensitization enables T cell responses to self-antigens. *J. Immunol.* **190**, 1416–1423 (2013).
42. D. I. Godfrey, H. F. Koay, J. McCluskey, N. A. Gherardin, The biology and functional importance of MAIT cells. *Nat. Immunol.* **20**, 1110–1128 (2019).
43. A. Toubal, I. Nel, S. Lotersztajn, A. Lehuen, Mucosal-associated invariant T cells and disease. *Nat. Rev. Immunol.* **19**, 643–657 (2019).

44. D. G. Pellicci, H. F. Koay, S. P. Berzins, Thymic development of unconventional T cells: How NKT cells, MAIT cells and gammadelta T cells emerge. *Nat. Rev. Immunol.* **20**, 756–770 (2020).
45. N. Tickotsky, T. Sagiv, J. Prilusky, E. Shifrut, N. Friedman, McPAS-TCR: A manually curated catalogue of pathology-associated T cell receptor sequences. *Bioinformatics* **33**, 2924–2929 (2017).
46. J. Wu *et al.*, Expanded TCRbeta CDR3 clonotypes distinguish Crohn's disease and ulcerative colitis patients. *Mucosal Immunol.* **11**, 1487–1495 (2018).
47. P. Parronchi *et al.*, Type 1 T-helper cell predominance and interleukin-12 expression in the gut of patients with Crohn's disease. *Am. J. Pathol.* **150**, 823–832 (1997).
48. Z. Liu *et al.*, IL-15 is highly expressed in inflammatory bowel disease and regulates local T cell-dependent cytokine production. *J. Immunol.* **164**, 3608–3615 (2000).
49. S. T. Leach *et al.*, Local and systemic interleukin-18 and interleukin-18-binding protein in children with inflammatory bowel disease. *Inflamm. Bowel Dis.* **14**, 68–74 (2008).
50. T. Sathaliyawala *et al.*, Distribution and compartmentalization of human circulating and tissue-resident memory T cell subsets. *Immunity* **38**, 187–197 (2013).
51. W. J. Sandborn *et al.*, Etrolizumab for the treatment of ulcerative colitis and Crohn's disease: An overview of the phase 3 clinical program. *Adv. Ther.* **37**, 3417–3431 (2020).
52. A. Sledzinska *et al.*, Regulatory T cells restrain Interleukin-2- and Blimp-1-dependent acquisition of Cytotoxic function by CD4(+) T cells. *Immunity* **52**, 151–166.e156 (2020).
53. H. Okamura *et al.*, Cloning of a new cytokine that induces IFN-gamma production by T cells. *Nature* **378**, 88–91 (1995).
54. T. Yoshimoto *et al.*, IL-12 up-regulates IL-18 receptor expression on T cells, Th1 cells, and B cells: Synergism with IL-18 for IFN-gamma production. *J. Immunol.* **161**, 3400–3407 (1998).
55. S. Fais *et al.*, Spontaneous release of interferon gamma by intestinal lamina propria lymphocytes in Crohn's disease. Kinetics of in vitro response to interferon gamma inducers. *Gut* **32**, 403–407 (1991).
56. I. J. Fuss *et al.*, Disparate CD4+ lamina propria (LP) lymphokine secretion profiles in inflammatory bowel disease. Crohn's disease LP cells manifest increased secretion of IFN-gamma, whereas ulcerative colitis LP cells manifest increased secretion of IL-5. *J. Immunol.* **157**, 1261–1270 (1996).
57. F. Powrie *et al.*, Inhibition of Th1 responses prevents inflammatory bowel disease in scid mice reconstituted with CD45RBhi CD4+ T cells. *Immunity* **1**, 553–562 (1994).
58. R. Ito *et al.*, Interferon-gamma is causatively involved in experimental inflammatory bowel disease in mice. *Clin. Exp. Immunol.* **146**, 330–338 (2006).
59. P. Nava *et al.*, Interferon-gamma regulates intestinal epithelial homeostasis through converging beta-catenin signaling pathways. *Immunity* **32**, 392–402 (2010).
60. Y. Eriguchi *et al.*, Essential role of IFN-gamma in T cell-associated intestinal inflammation. *JCI Insight* **3**, e121886 (2018).
61. L. Haep *et al.*, Interferon gamma counteracts the angiogenic switch and induces vascular permeability in dextran sulfate sodium colitis in mice. *Inflamm Bowel Dis.* **21**, 2360–2371 (2015).
62. V. Langer *et al.*, IFN-gamma drives inflammatory bowel disease pathogenesis through VE-cadherin-directed vascular barrier disruption. *J. Clin. Invest.* **129**, 4691–4707 (2019).
63. H. M. van Dullemen *et al.*, Treatment of Crohn's disease with anti-tumor necrosis factor chimeric monoclonal antibody (cA2). *Gastroenterology* **109**, 129–135 (1995).
64. T. Feng *et al.*, Th17 cells induce colitis and promote Th1 cell responses through IL-17 induction of innate IL-12 and IL-23 production. *J. Immunol.* **186**, 6313–6318 (2011).
65. S. N. Harbour, C. L. Maynard, C. L. Zindl, T. R. Schoeb, C. T. Weaver, Th17 cells give rise to Th1 cells that are required for the pathogenesis of colitis. *Proc. Natl. Acad. Sci. U.S.A.* **112**, 7061–7066 (2015).
66. Q. Yu *et al.*, T cell factor 1 initiates the T helper type 2 fate by inducing the transcription factor GATA-3 and repressing interferon-gamma. *Nat. Immunol.* **10**, 992–999 (2009).
67. N. Jaeger *et al.*, Single-cell analyses of Crohn's disease tissues reveal intestinal intraepithelial T cells heterogeneity and altered subset distributions. *Nat. Commun.* **12**, 1921 (2021).
68. T. Castro-Dopico *et al.*, Anti-commensal IgG drives intestinal inflammation and Type 17 immunity in ulcerative colitis. *Immunity* **50**, 1099–1114.e1010 (2019).
69. T. Mitsuishi, Correlation between histological findings and endoscopic findings in patients with ulcerative colitis: Basal plasmacytosis is an important finding suggesting active inflammation. *JGH Open* **3**, 100–104 (2019).